Received March 22, 2022, accepted March 31, 2022, date of publication April 6, 2022, date of current version April 14, 2022.

Digital Object Identifier 10.1109/ACCESS.2022.3165183

A Novel AC/DC Power Flow: HVDC-LCC/VSC Inclusion Into the PFPD Bus Admittance Matrix

ROBERTO BENATO, (Senior Member, IEEE), AND GIOVANNI GARDAN, (Member, IEEE)
Department of Industrial Engineering, University of Padova, 35131 Padova, Italy
Corresponding author: Roberto Benato (roberto.benato@unipd.it)

ABSTRACT In this paper, the matrix algorithm PFPD is generalized in order to compute the power flow solution of real and large AC/DC transmission networks. In particular, it is demonstrated that the HVDC-VSC/LCC links can be seen from the AC power systems as PV/PQ constraints, which englobe both the AC and DC characteristics of the HVDC links. The proposed analytical formulation to assess the PV/PQ constraints is valid for any other numerical methods (*e.g.,* Newton-Raphson and derived, Gauss-Seidel, *etc.*). Furthermore, an iterative procedure for estimating the reactive power absorption of HVDC-LCC links from the power system is proposed. In order to validate the algorithm, solution comparisons with the commercial software DIgSILENT PowerFactoy are presented. This validation procedure shows that the algorithm can analyse large and real HVAC/HVDC networks (*e.g.*, the Italian transmission one with its five HVDC links). Therefore, the conciseness, accuracy and performances of PFPD for studying real and large AC/DC power systems is confirmed.

INDEX TERMS AC/DC power flow, admittance matrix power flow, HVDC-VSC, HVDC-LCC, AC/DC Italian transmission network.

A. SETS AND INDICES

sched	Scheduled quantity.
conv	Quantity related to the converter.
loss	Loss term.
loss_switch	Switching loss term.
loss_conv	Converter loss term.
loss_line	Line loss term.
$P_{no,load}$	No-load loss factor.
$G_{no,load}$	No-load conductive coefficient.
S	Transmitter converter station.
R	Receiver converter station.
LL	Line-to-line.
$\underline{\mathbf{Y}}_{\mathbf{SGL}}$	Total bus admittance used in PFPD.
i	Generic i-th element/node.
n	Network number of nodes.
$a \div g$	Set of generators.
$h \div m$	Set of loads.

B. VARIABLES AND PARAMETERS

j	Imaginary unit.
V	AC voltage module *or* DC voltage.
L_S	Equivalent AC network inductance.
I	AC current module *or* DC current.
r	Kilometric DC line resistance.
$\underline{y}$	Complex admittance.
n_S	Number of PV/PQ constraints modelling the sending converter station.
n_R	Number of PV/PQ constraints modelling the receiving converter station.
n_L	Point-to-point HVDC link number of DC lines.
ℓ	DC line length.
P	Active power.
Q	Reactive power.
S	Apparent power.
ϑ	LCC converter control angle.
α	LCC converter delay firing angle.
β	LCC converter leading firing angle.
γ	LCC converter leading extinction angle.
μ	LCC converter commutation angle.
tol	IRPE voltage tolerance.
k'	Switching loss factor.
k''	Resistive loss factor.

C. SYMBOLS

$\div$	From . . . to . . .

The associate editor coordinating the review of this manuscript and approving it for publication was Youngjin Kim.

D. ACRONYMS

HVDC	**H**igh **V**oltage **D**irect **C**urrent.
HV	**H**igh **V**oltage.
EHV	**E**xtra **H**igh **V**oltage.
PCC	**P**oint of **C**ommon **C**oupling.
VSC	**V**oltage **S**ource **C**onverter.
LCC	**L**ine **C**ommutated **C**onverter.
RPC	**R**eactive **P**ower **C**ontrol.
AC	**A**lternate **C**urrent.
RMS	**R**oot **M**ean **S**quare.
DPF	**D**isplacement **P**ower **F**actor.
DC	**D**irect **C**urrent.
IRPE	**I**terative **R**eactive **P**ower **E**stimation.
DGS	**DIgSI**LENT PowerFactory.
PFPD	**P**ower **F**low of the University of **P**a**d**ova.
F.I.L.	**F**rance-**I**taly **L**ink.
SA.CO.I.	**SA**rdinia **CO**rsica **I**taly.
SAPE.I.	**SA**rdinia **PE**ninsula **I**taly.
GR.ITA	**GR**eece-**ITA**ly.
MON.ITA	**MON**tenegro-**ITA**ly.

I. INTRODUCTION

A. MOTIVATIONS

In 2022, Roberto Benato published a novel AC matrix power flow algorithm named as PFPD [1]. This algorithm is based on an extensive use of the bus admittance matrix including generators, loads, and also the slack generator: the theoretical possibility of modelling the slack generator as a quasi-ideal current one gives a very easily-implementable, efficient and fast algorithm for AC networks.

Notwithstanding, the paper [1] does not deal with the AC/DC power flow problem *i.e.*, the compresence of both HVDC-VSC and HVDC-LCC point-to-point links inside an AC power system.

This problem arises since the compresence of HVDC-LCC/VSC links in HV and EHV transmission networks is an increasingly widespread reality. In fact, in some contexts, several reasons make the HVDC technologies preferable to HVAC ones, such as: the greater interconnection capacity [2], [3]; the more economical, reliable, and sustainable operation [4]–[6]; and the possibility to integrate large scale of Renewable Energy Sources (RES) in power systems [7].

Therefore, it is firstly necessary to have powerful tools to compute the power flow solution of such AC/DC networks for steady-state operation evaluations, contingency analyses, and planning. Moreover, the power flow evaluation is the initial necessary step to make dynamic evaluations [8]. By considering all the implementation, computational, and research advantages of [1], a general formulation of PFPD can be a valid alternative to the Newton-Raphson formulations to compute AC/DC power flow.

This paper proposes a matrix power flow formulation for solving the AC/DC power flow problem efficiently by means of PFPD.

B. LITERATURE REVIEW

After the first HVDC industrial application in 1954, investigations on power flow formulations for networks containing HVDC links started in the 1960s [9]–[12]. All the methods in [9]–[12] use the Newton-Raphson approach to solve the non-linearity of the power flow problem. In such contributions, the DC and AC systems are treated separately and not solved simultaneously: this choice makes the approach inefficient. In [13], [14], the AC and DC equations are formulated simultaneously, therefore a unique Jacobian matrix is adopted.

Although the first power flow methods were matrix ones [15], [16], such approaches have been never adopted to solve the AC/DC power flow problem. The matrix approaches, in fact, are long abandoned. In [1], however, the strengths of matrix approaches for power flow purposes are highlighted.

Until the 1990s, the AC/DC power flow formulations in power systems with HVDC links consider only the HVDC-LCC technologies (which is the first-appeared HVDC technology). After the first experimental applications in the late 1990s of the HVDC-VSC model [17], [18] proposes a research modelling of such devices for power flow purposes [19]–[22]. In particular, the converters can control the active and reactive power independently. This greater controllability makes the power flow formulation more flexible.

C. CONTRIBUTIONS

In this paper, it is demonstrated that PFPD can be generalised for assessing the steady-state regime of modern AC/DC transmission networks. Therefore, PFPD is intended as the *first iterative matrix method* to solve the AC/DC power flow problem for transmission networks (different formulation from the well-known numerical methods *e.g.* Newton-Raphson, decoupled approaches, Gauss-Seidel, etc.). In fact, once the typical HVDC controlled variables are fixed, the classical PV/PQ constraint formulation is valid for modelling point-to-point HVDC links.

In particular, the HVDC-VSC links are modelled as PV constraints (they can also be modelled as PQ constraints, since the active and reactive power can be controlled independently), whereas HVDC-LCC links are modelled as PQ ones. Since, in LCC devices, the absorption of reactive power cannot be controlled independently from the active one, an iterative procedure (IRPE) estimating the reactive power absorption of the LCC converter for power flow purposes is presented. Therefore, the AC/DC power flow formulation can be reduced to an AC one, and the HVDC information is englobed in the ''all-inclusive'' admittance matrix of PFPD [1]. As a consequence, the DC variables quantities disappear from the iterative formulation, but their impact into the AC system is correctly assessed (*e.g.,* global power loss computation). Notwithstanding, the actual DC values of voltages and currents can be computed normally. It is worth noting that such way of modelling an AC/DC network as an AC one is

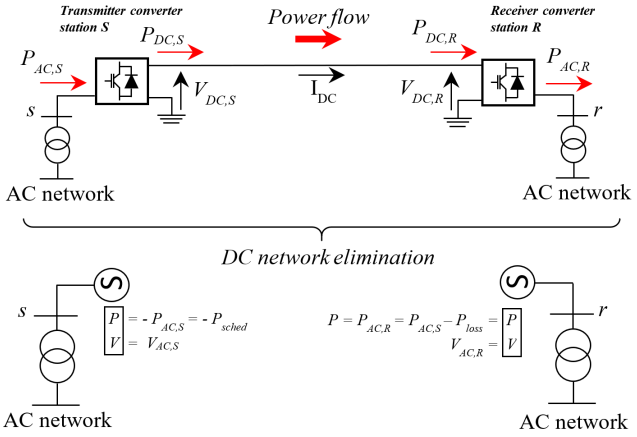

FIGURE 1. Monopolar HVDC-VSC link treatment by means of PV constraints: the DC network is eliminated, even if its effect is considered in the PV constraints.

general, so it can be exploited for all the classical numerical methods (*e.g.* Newton-Raphson, decoupled approaches, Gauss-Seidel, etc.).

Eventually, some solution comparisons with the commercial software DGS are presented in order to validate the proposed method. In particular, the algorithm is tested by the Italian network, which has got five HVDC links (four with foreign nations), in order to ensure the applicability of PFPD to a real and large transmission network.

II. PFPD HVDC MODELLING BY MEANS OF THE DC ELIMINATION TECHNIQUE

In this study, a suitable modeling of both the HVDC-VSC (see Sect. III) and HVDC-LCC (see Sect. IV) technologies for PFPD is presented.

The HVDC links are modelled by means of PV or PQ constraints to be embedded inside the ''all-inclusive'' matrix $\underline{\mathbf{Y}}_{\mathbf{SGL}}$ [1]. Obviously, such PV and PQ constraints do not represent the synchronous generators and the loads respectively, as in the classical AC power flow problem. However, they suitably assess the impact of the point-to-point HVDC technologies in the power system from a steady-state point of view. Moreover, the station converters and the DC link are not directly represented, but their presence is taken into account when the PV/PQ formulation (this fact is indicated as ''DC elimination technique'').

Although the converters introduce voltage/current harmonics in the power system, a ''fundamental frequency model'' approach is adopted, since the power flow problem is related to the power system fundamental frequency. In fact, the filters on both AC and DC sides cancel the harmonic power contribution.

However, the impact of the filters for harmonic compensations is taken into accont at the fundamental frequency only. In particular, the power losses due to current absorption in such devices is computable.

Eventually, HVDC converters are usually connected with OLTC transformers, which allows controlling the AC secondary voltage and so the DC link voltage (together with the angle α). Such elements are implemented and their modelling is described in [1].

III. HVDC-VSC LINK MODELLING

A. THE TRANSMITTER STATION MODELLING (PV-CONSTRAINT MODELLING)

The VSC transmitter converter can control both the AC terminal voltage and the transmissible active power.

Fig. 1 shows a monopolar HVDC-VSC link supplied by two-winding transformers.

The power flow direction conventionally goes from the transmitter converter (S) to the receiver one (R). The transmitter converter S is controlled to absorb, from the AC network, a scheduled active power to be transmitted *i.e.,*

$$P_{AC,S} = P_{sched}.$$

In fact, in VSC converters, the voltage phasor position can be controlled with respect to the network one. Moreover, the voltage value at its AC terminal can be scheduled:

$$V_{AC,S} = V_{sched}$$

Thus, the AC terminal of the VSC transmitter converters can be set as PV constraint, where $P = -P_{sched}$ and $V = V_{sched}$. The negative sign of P is due to the fact that the transmitter converter absorbs (and does not inject) active power from the network (active sign convention for PV constraints).

B. THE RECEIVER STATION MODELLING (PV-CONSTRAINT MODELLING)

The receiver converter typically controls both the AC and the DC terminal voltages:

$$V_{AC,R} = V_{AC,sched}$$
$$V_{DC,R} = V_{DC,sched}$$

The voltage $V_{DC,R}$, in fact, must be controlled and kept constant for two reasons: ensuring both the proper operation (V_{DC} smooth voltage) of the VSC converters and the active power balancing from the transmitter to the receiver converter.

The receiver converter R converts the DC-bus power $P_{DC,R}$ into the AC active power $P_{AC,R}$, which can be computed by knowing the active power losses P_{loss} occurring in the VSC converters and in the DC line:

$$P_{AC,R} = P_{sched} - P_{loss}. \quad (1)$$

The expression of P_{loss} is the following:

$$P_{loss} = P_{loss\_conv,S} + P_{loss\_conv,R} + P_{loss\_line} \quad (2)$$

where $P_{loss\_conv,S}$ and $P_{loss\_conv,R}$ represent the losses due to converter S and R respectively, whereas P_{loss_line} is due to the Joule losses in the DC line.

The value of the Joule losses in the DC line can be computed by considering the current I_{DC}:

$$P_{loss\_line} = r \cdot \ell \cdot {I_{DC}}^2. \quad (3)$$

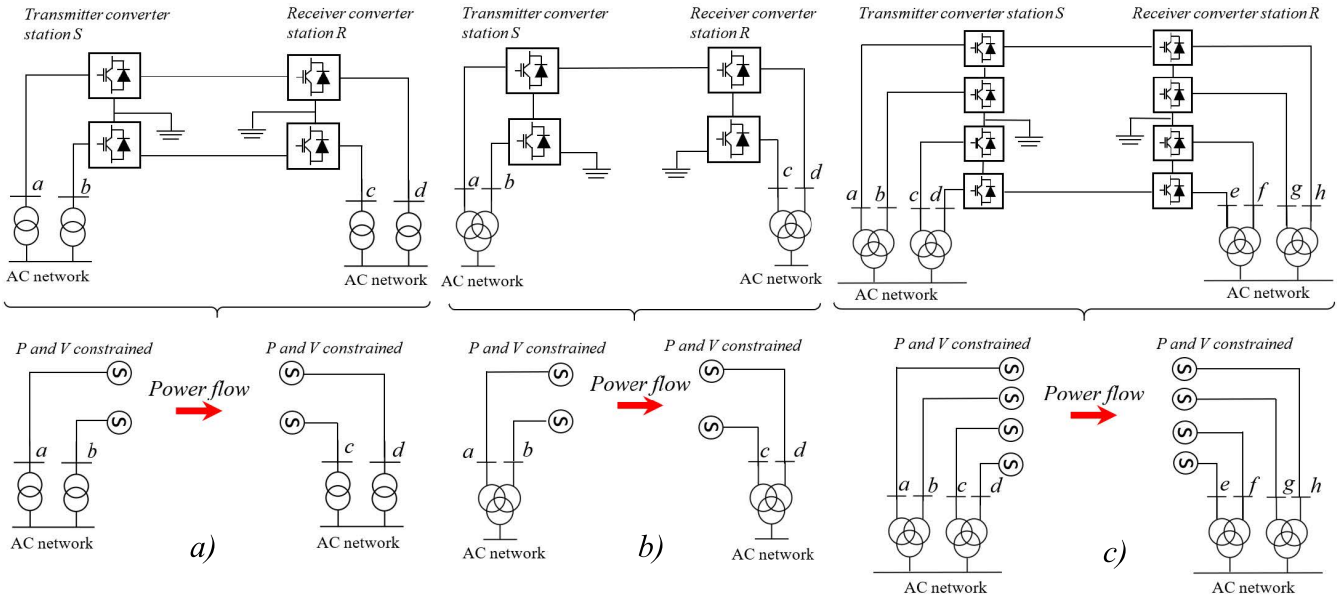

FIGURE 2. Possible HVDC-VSC configurations and their modelling by means of PV constraints.

TABLE 1. Converter loss term symbols, descriptions and their associated loss factors.

Symbol	Description	Loss factor
P_{loss_noload}	No-load losses	$P_{no,load}$ [kW]
P_{loss_switch}	Switching losses	k' [kW/A]
P_{loss_cond}	Resistive losses	k'' [Ω]

By considering the "fundamental frequency model" approach, the losses of each converter are given by the sum of three terms [23]:

$$P_{loss\_conv} = P_{loss\_noload} + P_{loss\_switch} + P_{loss\_cond} \tag{4}$$

where P_{loss_noload} represents the no load loss contribution, P_{loss_switch} represents the switching loss contribution and P_{loss_cond} represents the resistive loss contribution.

As shown in Table 1, for each term of the right-hand side of (4), an input loss factor is defined: $P_{no,load}$ for the no load losses, k' for the switching losses and k'' for the resistive losses. Thus the addends of (4) can be computed by knowing such loss factors characteristic of the converter [24].

For the no-load losses P_{loss_noload}, the conductance coefficient G_{no_load} must be computed by knowing the its input loss factor $P_{no,load}$ [MW] and the DC rated voltage [kV] as follows [24]:

$$G_{no\_load} = \frac{P_{no,load}}{1000\ U^2_{DC,nom}}. \tag{5}$$

Therefore, the no-load losses, P_{loss_noload}, can be computed:

$$P_{loss\_noload} = G_{no\_load} U^2_{DC} \tag{6}$$

The switching losses, P_{loss_switch}, depend on the current I_{DC} circulating in the DC line as follows:

$$P_{loss\_switch} = V_{drop} \cdot I_{DC} \tag{7}$$

where the coefficient V_{drop} is:

$$V_{drop} = \text{sign}(I_{DC}) \cdot k' \cdot (1 - e^{-200 \cdot I_{DC}}) \tag{8}$$

and k' is the loss factor characterising the switching losses per unit current. The resistive losses P_{loss_cond} can be computed according to the following relation:

$$P_{loss\_cond} = k'' \cdot I^2_{DC} \tag{9}$$

where k'' is the resistive loss input factor.

In order to compute I_{DC}, the following system is considered:

$$\begin{cases} P_{AC,S} - P_{loss\_conv,S} = I_{DC} \cdot V_{DC,S} \\ V_{DC,S} = V_{DC,R} + r \cdot \ell \cdot I_{DC} \end{cases} \tag{10}$$

which leads to:

$$I^2_{DC}(r \cdot \ell + k'') + I_{DC}(V_{DC,R} + V_{drop}) + P_{loss\_noload,S} - P_{AC,S} = 0 \tag{11}$$

Therefore, once the controlled variables are fixed, I_{DC} is a term computable *a priori* (*i.e.,* before the power flow computation) by means of (11). By considering the set of equations (2)÷(9), the value I_{DC} allows determining P_{loss}. Therefore the PV active power constraint of the receiver converter AC terminal can be computed by means of (1).

It is worth underlying that modelling the transmitter and receiver converters by means of conventional PV constraints allows finding the AC-side converter phase angles as the solution of the power flow problem.

By extending the above-mentioned procedure, the following HVDC-VSC typical configurations [2] can be immediately modelled:

- Type 1: Monopolar HVDC-VSC supplied by two winding transformers (see Fig. 1),

- Type 2: Bipolar HVDC-VSC supplied by two winding transformers (see Fig. 2a)),
- Type 3: Monopolar HVDC-VSC supplied by three winding transformers (see Fig. 2b)),
- Type 4: Bipolar HVDC-VSC supplied by three winding transformers (see Fig. 2c)).

As it can be seen in Fig. 2, every AC converter terminal is considered as a PV constraint. Therefore, multibridge converter configurations can be studied, by using one PV constraint for each converter. However, in industrial reality, for high power transmission the double-bridge solution is the most used in order not to complicate the DC control [25].

The schedule active power of the sending converter station S can be equally considered shared among the different n_S PV constraints. Therefore, the power of the sending i-th PV constraint which models the i-th converter is:

$$P_{AC,S(i)} = P_{sched}/n_S,$$

each of which is characterised by the corresponding scheduled AC voltage:

$$V_{AC,S(i)} = V_{sched,S(i)}.$$

With regard to the constraints of the receiving converter, (2) can be generalised in the following:

$$P_{loss} = \sum_{i=1}^{n_S} P_{loss\_conv,S,i} + \sum_{i=1}^{n_R} P_{loss\_conv,R,i} + \sum_{i=1}^{n_L} P_{loss\_line,i}. \quad (12)$$

Therefore, by subdividing the global losses of (12) for all the receiving PV constraints, the active power of the i-th PV receiving constraint is:

$$P_{AC,R(i)} = P_{\text{sched}}/n_R - P_{loss}/n_R \quad (13)$$

each of which is characterised by the AC voltage controlled by the corresponding converter:

$$V_{AC,R(i)} = V_{sched,R(i)} \quad (14)$$

C. HVDC-VSC LINKS (PQ CONSTRAINTS)

Since active and reactive power can be independently controlled, the VSC converters can be also modelled as PQ nodes, where P and Q are the scheduled power values.

In this way of modelling, the AC-bus converter voltage magnitude cannot be controlled and depends on the power flow solution. Therefore, this control mode can be used only if it is assured that the active and reactive power assume values not causing high voltage drops on the VSC converter AC bus node (strong AC network as seen from the AC-bus converter). Hence, this control mode has got effects which are different from the VSC converter modelling meant as PV constraints, where the voltage magnitude is set (but not the reactive power).

The active power loss computation is the same of the one described in sub-section B.

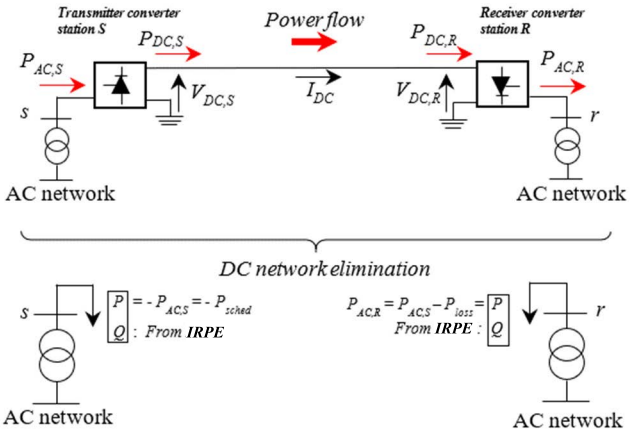

FIGURE 3. Transformation of an HVDC-LCC monopolar link to PQ constraints, by means of the DC elimination technique.

IV. HVDC-LCC LINKS MODELLING

A. THE TRANSMITTER STATION MODELLING (PQ-CONSTRAINT MODELLING)

Fig. 3 shows a basic monopolar HVDC-LCC configuration introducing the concept of PQ-constraint modelling of such technology. These PQ constraints model the active and reactive HVDC power absorptions as seen from the AC network: the impact of the DC links can be assessed by considering only their AC converter terminals.

The transmitter converter controls the transmittable DC power. In fact, under the hypothesis of constant current I_{DC}, the value of the DC voltage can be controlled through the delay firing angle α ($0° < \alpha < 90°$) as it follows [23]:

$$V_{DC,S} = \frac{3 \cdot \sqrt{2}}{\pi} \cdot V_{LL,S} \cdot \cos\alpha - \frac{3\omega L_s}{\pi} I_{DC} + k'' I_{DC} + V_{drop} \quad (15)$$

where the coefficients k'', V_{drop} assume the same meaning already explained for VSC converters [23]. Eq. (15) is valid for both inverter and rectifier operation modes and take into account the loss contribution.

Therefore, it is possible to transmitt the scheduled DC power from the trasmitter convert station, *i.e.*,

$$P_{DC,sched} = P_{DC,S} = V_{DC,S} \cdot I_{DC}. \quad (16)$$

In order to compute I_{DC}, the following system is considered:

$$\begin{cases} P_{sched} = V_{DC,S} \cdot I_{DC} \\ V_{DC,S} = V_{DC,R} + r \cdot \ell \cdot I_{DC} \end{cases} \quad (17)$$

which leads to:

$$r \cdot \ell \cdot I_{DC}^2 + V_{DC,R} I_{DC} - P_{DC,sched} = 0, \quad (18)$$

Thus, it is possible to find I_{DC}.

Similarly to the VSC case, once the controlled variables are fixed, I_{DC} is a term computable *a priori* (*i.e.,* before the power flow computation).

The transmitter converter absorbs both active and reactive power from the network, so it is possible to define a PQ

constraint at its AC terminal. The AC active power absorption of the transmitter converter depends on the active power losses in the converter S:

$$P_{AC,S} = P_{DC,sched} + P_{loss\_conv,S}. \tag{19}$$

According to the loss computing approach of [23], for the thyristor converters, the relations (5)÷(9) are still valid. Therefore, the active power absorbed of (19) as seen from the AC LCC rectifier terminal can be computed.

For the reactive power computation, see subsection C) of the present section.

B. THE RECEIVER STATION MODELLING

The receiver converter R converts the DC bus power $P_{DC,R}$ into the AC active power $P_{AC,R}$: the converter operates in the inverter mode ($90° < \alpha < 180°$ and $\alpha < 180°$-γ to avoid commmutation failure [26]). In the inverter operation, the active power transmitted in the AC network depends on the DC line and on the converter R:

$$P_{AC,R} = -(P_{DC,sched} - P_{loss\_conv,R}) < 0 \tag{20}$$

where the formulations (3)÷(9) are still valid. It is worth noting the negative sign of $P_{AC,R}$, since the positive power is injected into the network. As it is explained in sub-section C), the inverter reactive power computation is the same of the rectifier one. By extending the above-mentioned procedure, four different HVDC-LCC configurations are modelled (see Fig. 4):

- Type 1: HVDC-LCC monopolar, supplied by two winding transformers (see Fig. 3)
- Type 2: HVDC- LCC bipolar, supplied by two winding transformers (see Fig. 4 a)
- Type 3: HVDC- LCC monopolar, supplied by three winding transformers (see Fig. 4 b)
- Type 4: HVDC- LCC bipolar, supplied by three winding transformers (see Fig. 4 c)

As it can be seen in Fig. 4, every AC converter terminal is considered as a PQ constraint. As for VSC, multibridge converter configurations can be studied, by using one PQ constraint for each converter. The active power of each sending converter station S can be computed by equally dividing $P_{DC,sched}$ into n_S converters:

$$P_{DC,S(i)} = P_{DC,sched}/n_S,$$

and then by applying (19) for each i-th converter. In order to model the active power injected by the receiving converters, the sum of the losses in all the lines and receiving converters must be taken into account:

$$P_{loss} = \sum_{i=1}^{n_R} P_{loss\_conv,R} + \sum_{i=1}^{n_L} P_{loss\_line}. \tag{21}$$

Therefore, by subdividing the global losses of (21) for all the receiving PQ constraints, the active power of the i-th PV receiving constraint is:

$$P_{AC,R(i)} = -(P_{sched}/n_R - P_{loss}/n_R) \tag{22}$$

The negative sign of (22) is due to the fact that the PQ constraint is injecting active power. The reactive power computation for both the rectifier/inverter converters is estimated by means of the **IRPE** method, described in the following sub-section.

C. THE IRPE METHOD: THE LCC REACTIVE POWER ABSORPTION COMPUTATION

In this subsection, a method to estimate the LCC reactive power absorptions for power flow purposes is presented.

Firstly, it is assumed that the commutation reactance and the converter losses are negligible. The reactive power absorbed by an LCC converter depends on its control angle ϑ. This angle corresponds to the delay firing angle α for a rectifier and to the leading firing angle β for an inverter (hence, $0° < \vartheta < 90°$).

By considering an LCC converter, the following relation is valid:

$$Q \cong |P| \cdot \tan(\vartheta) \tag{23}$$

where Q is the reactive power set absorbed by the converter and P is alternativelly the active power absorbed from the AC system (for rectifiers) or injected into the AC system (for inverters).

Differently from the VSC case, the LCC converter AC side voltage cannot be controlled, since it depends on the power flow solution, and the value of ϑ is set to control the active power. Therefore, the value of the reactive power Q computable by means of (20), cannot be controlled *a priori*, but it is a function of the power flow problem.

In order to compute the reactive power Q, it is possible to proceed iteratively.

By considering an LCC converter (a rectifier or an inverter), its reactive power absorption is

$$Q_{conv} = \sqrt{S^2 - P_{sched}^2} \tag{24}$$

thus

$$Q_{conv} = \sqrt{(\sqrt{3}\, V_{AC} I_{AC})^2 - P_{sched}^2} \tag{25}$$

and by substituting the relation between the DC current and the AC one [26]

$$I_{AC} = \frac{\sqrt{6}}{\pi} I_{DC} \tag{26}$$

in (25), the expression (27) for the reactive power computation can be derived:

$$Q_{conv} = V_{AC} \sqrt{\frac{18}{\pi^2} I_{DC}^2 - \left(\frac{P_{sched}}{V_{AC}}\right)^2}, \tag{27}$$

which basically links the reactive power Q_{conv} with the unknown AC voltage module V_{AC}. The values of I_{DC} and P_{sched} are constant (I_{DC} is computable a priori by solving (18) and P_{sched} is the controlled quantity). It is worth noting that Q_{conv} is always positive for both rectifier and inverter.

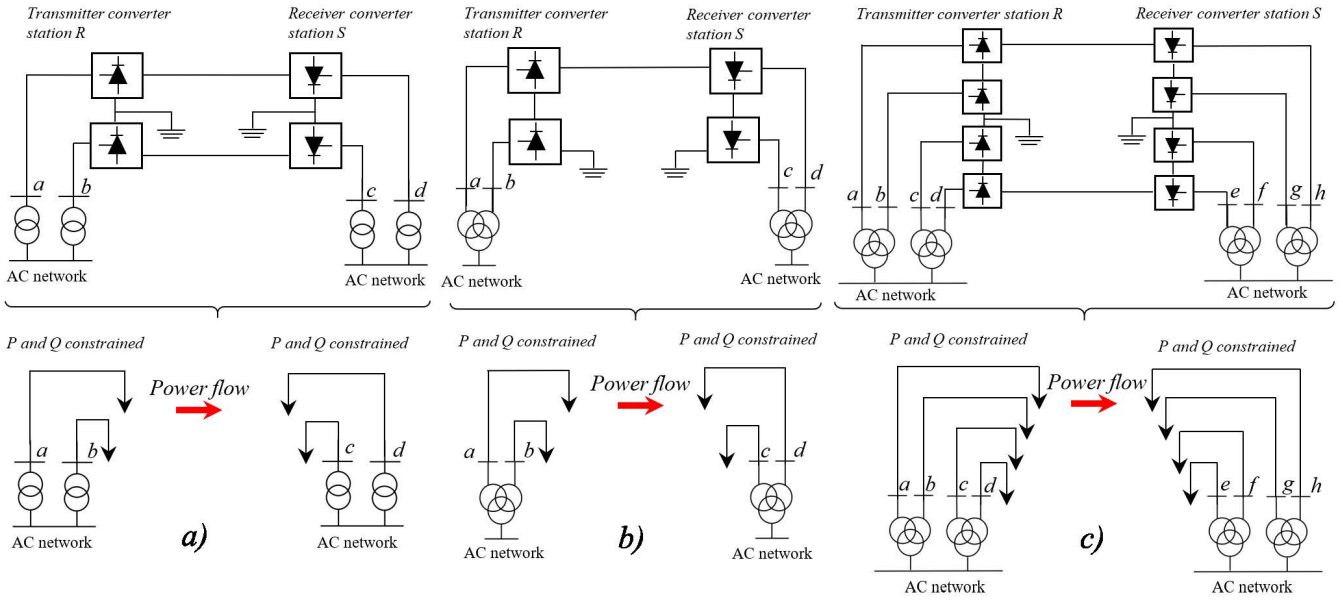

FIGURE 4. Possible HVDC-LCC configurations and their modelling by means of PQ constraints.

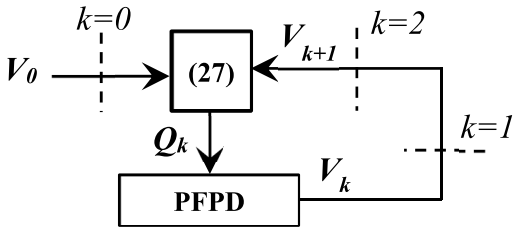

FIGURE 5. Flow chart for the reactive power estimation technique (IRPE method).

Formulation (27) is suitable to be computed iteratively as a cycle external to the PFPD.

The initial guess for the AC voltage module of the converter is set to 1 p.u. This value is near to the power flow solution since, for transmission purposes, LCC converters ought to be connected to strong AC nodes.

By substituting this initial guess in (27), an estimation of the reactive power Q_{conv} is obtained. Therefore, the LCC converter can be modelled as PQ nodes, where $Q = Q_{conv}$. Eventually the PFPD computation update the voltage module of the converter. Therefore (27) can be applied again, and the procedure is iteratively repeated (see Fig. 5) until the mismatch between the voltage module of two consecutive iterations is less than a predifinied tolerance *tol*:

$$\Delta V_k = V_k - V_{k-1} < tol. \tag{28}$$

In this study, a typical value for this voltage tolerance *tol* is equal to 100 V. The present procedure can be summarized and visualized by considering the flow chart of Fig. 5. Such iterative procedure can be written in matrix formulation (vectorization), thus it is possible to consider all the HVDC link reactive power updates simultenously.

This reactive power estimation is named as **IRPE** (**I**terative **R**eactive **P**ower **E**stimation). The method presented is valid for LCC converters operating both in inverter and rectifier mode (both the operation modes need to absorb positive reactive power from the AC system) [27].

V. INSERTION OF THE HVDC-VSC/LCC POWER FLOW CONSTRAINTS INSIDE $\mathbf{Y_{SGL}}$

In PFPD the PV constraints modelling the HVDC-VSC links are modelled as passive admittances [1] as in the following:

$$\underline{y}_i = -\frac{P_i}{V_i^2} + j\frac{Q_i}{V_i^2}, \tag{29}$$

where $i \in a \div g$.

The admittance $\underline{y}_i$ is positioned in the PV submatrix, P_i and V_i are fixed in accordance with the procedure of Sect. III A and III B, and Q_i is the unknown reactive power absorbed by the HVDC-VSC link.

Once the PV constraint admittances are computed, they can be embedded in the i-th diagonal position of the square $\underline{\mathbf{Y}}_{\mathbf{SGL}}$ admittance matrix (see Fig. 6a). It is worth noting that in such admittances the reactive power estimation is the same as that for estimating reactive power of the conventional AC generators in PFPD [1].

Similarly, the PQ constraints modeling the HVDC-LCC links are modelled as passive admittances by means of (30):

$$\underline{y}_i = \frac{P_i}{V_i^2} - j\frac{Q_i}{V_i^2}. \tag{30}$$

where $i \in h \div m$. $\underline{y}_i$ is positioned in the PQ submatrix P_i and Q_i are fixed and computed according to the procedure of Sect. IV A/IV B and Sect. IV C. It is worth noting the opposite signs of the expressions (29), (30). Q_i is the unknown reactive power absorbed by the HVDC link.

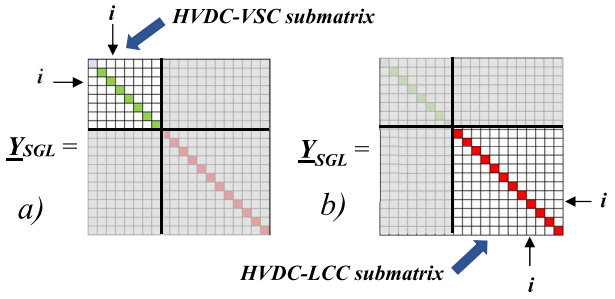

FIGURE 6. PV and PQ position in the matrix $\underline{\mathbf{Y}}_{\mathbf{SGL}}$ constraints modelling the HVDC-VSC-LCC constraints.

Once the PQ constraint admittances are computed, they are embedded in the i-th diagonal position of the square $\underline{\mathbf{Y}}_{\mathbf{SGL}}$ admittance matrix (see Fig. 6b).

Therefore, by considering a network with n buses, the dimension of the AC/DC problem is always described by an $(n \times n)$ $\underline{\mathbf{Y}}_{\mathbf{SGL}}$ matrix, which contains the HVDC information also by means of PV/PQ constraints.

This fact is valid independently from the number of HVDC links. Therefore, the insertion of further HVDC in an n-bus network does not increase the dimension of the problem.

It is of note that the elimination of the DC part can create different separated subsystems if the two connected systems by the HVDC link have no other connections between them [25]. However, this fact does not introduce any computational critical issue.

Hence, once the matrix $\underline{\mathbf{Y}}_{\mathbf{SGL}}$ containing HVDC information is built, the iterative procedure is the same of the AC situation.

Moreover, the modelling of the HVDC links by means of shunt admittances (and not branch admittances) makes the matrix further well-conditioned [1], [28], since such admittances are in the matrix diagonal position.

VI. THE DC QUANTITIES

By considering the typical converter control schemes adopted in the HVDC links and described in this paper, the DC quantities can be computed directly, without the need of using any iterative procedure.

For both the HVDC-LCC and VSC configurations, in fact, the transmitted active power and the DC voltage at the sending side are constant. As it is explained in Sect. II, the DC voltage of the receiver side converter is constant, whereas the current I_{DC} can be computed *a priori* by means of (11) and (18).

Therefore, the value of the sending DC voltage can be computed by considering the voltage drop due to the DC current circulation. In general, by considering the series of the converters at both side:

$$\sum_{i=1}^{n_S} V_{Si,DC} = \sum_{i=1}^{n_R} V_{DC,Ri} + \sum_{i=1}^{n_L} r_i \ell_i I_{DC} \tag{31}$$

where r_i and ℓ_i are the resistances and the lengths of the DC connection sections.

Eventually, the value of α for rectifiers and β for inverters can be computed by the knowledge of the AC active/reactive power absorbed by the converters after the power flow calculation.

VII. AC/DC POWER FLOW SIMULATIONS BY MEANS OF PFPD

PFPD is implemented in Matlab environment. In order to test its effectiveness in including HVDC links, solution comparisons with the commercial software DGS are shown.

All the HVDC connections of this paper (see Fig. 1, 2, 3, and 4) are considered one at a time.

After the computations, the power flow solutions in PFPD and DGS are compared in terms of voltage magnitude and angle. For the voltage magnitude, the following vector of the relative mismatch between PFPD and DGS solutions is computed:

$$\Delta \mathbf{V} = \left| \frac{\mathbf{V_{PFPD}} - \mathbf{V_{DGS}}}{\mathbf{V_{DGS}}} \right| \tag{32}$$

where $\mathbf{V_{PFPD}}$ and $\mathbf{V_{DGS}}$ are the voltage magnitude vectors, and $\Delta \mathbf{V}$ is the voltage magnitude mismatch vector.

For the voltage angles the following mismatch vector between the PFPD and DGS solutions is computed:

$$\Delta \boldsymbol{\delta} = |\boldsymbol{\delta}_{\mathbf{PFPD}} - \boldsymbol{\delta}_{\mathbf{DGS}}| \tag{33}$$

where $\boldsymbol{\delta}_{\mathbf{PFPD}}$ and $\boldsymbol{\delta}_{\mathbf{DGS}}$ are the angle magnitude vectors, and $\Delta \boldsymbol{\delta}$ is the angle magnitude mismatch vector.

A. VALIDATION OF PFPD: HVDC-VSC LINKS

The four HVDC-VSC configurations are inserted between buses 15 and 16 of the AC 18-bus test network (see App. I). Therefore, the following four test cases are analysed:

1. ***Case A:*** Network containing monopolar HVDC-VSC link supplied by two-winding transformers.
2. ***Case B:*** Network containing bipolar HVDC-VSC link supplied by two-winding transformers.
3. ***Case C:*** Network containing monopolar HVDC-VSC link supplied by three-winding transformers.
4. ***Case D:*** Network containing bipolar HVDC-VSC link supplied by three-winding transformers.

For each case, a power flow computation and solution comparison with DGS are performed. The tolerance of PFPD is set to 10^{-8} p.u.

Table 2 reports the order of magnitude of the maximum solution mismatches between PFPD and DGS computed by means of (32) and (33). Such values confirm the very good agreement between the two computational methods.

B. VALIDATION OF PFPD: HVDC-LCC LINKS

The four HVDC-LCC configurations are inserted between buses 15 and 16 of the AC 18-bus test network (see App. I). Therefore, the following four test cases are analysed:

1. ***Case E:*** Network containing monopolar HVDC-LCC link supplied by two-winding transformers.

TABLE 2. Solution maximum deviations (order of magnitude) between PFPD and DGS (tolerance 10^{-8} p.u.), considering the presence of HVDC-VSC links.

	$\Delta\delta$ [°]	ΔV [%]
Case A	10^{-5}	10^{-6}
Case B	10^{-1}	10^{-2}
Case C	10^{-1}	10^{-3}
Case D	10^{-1}	10^{-3}

TABLE 3. Solution maximum deviations (order of magnitude) between PFPD and DGS (tolerance 10^{-8} p.u.), considering the presence of HVDC-LCC links.

	$\Delta\delta$ [°]	ΔV [%]
Case E	10^{-4}	10^{-5}
Case F	10^{-2}	10^{-2}
Case G	10^{-1}	10^{-4}
Case H	10^{-1}	10^{-4}

TABLE 4. Solution maximum deviations (order of magnitude) between PFPD and DGS (tolerance 10^{-8} p.u.), considering the Compresence of HVDC-VSC/LCC links.

	δ [°]	ΔV [%]
Case I	10^{-2}	10^{-4}
Case L	10^{-1}	10^{-1}
Case M	10^{-2}	10^{-2}

2. ***Case F:*** Network containing bipolar HVDC-LCC link supplied by two-winding transformers.
3. ***Case G:*** Network containing monopolar HVDC-LCC link supplied by three-winding transformers.
4. ***Case H:*** Network containing bipolar HVDC-LCC link supplied by three-winding transformers.

The tolerance of PFPD is set to 10^{-8} p.u. Since in such test networks, there are HVDC-LCC links, a tolerance for the IRPE method equal to 100 V is fixed. Table 3 reports the order of magnitude of the maximum solution mismatches between PFPD and DGS computed by means of (32) and (33). Also in this case, the values confirm the very good agreement between the two computational methods.

C. VALIDATION OF PFPD: COOPERATIOON OF HVDC-VSC AND HVDC-LCC LINKS

In this section, the possibility of computing the power flow solution by considering more HVDC links in the same network is assessed. A 60-bus fictitious network is considered and the three following cases are studied:

1. ***Case I:*** Network containing a monopolar HVDC-VSC link supplied by two-winding transformers and a bipolar HVDC-VSC link supplied by three-winding transformers.
2. ***Case L:*** Network containing a monopolar HVDC-LCC link supplied by two-winding transformers and a bipolar HVDC-LCC link supplied by three-winding transformers.
3. ***Case M:*** Network containing a bipolar HVDC-VSC link supplied by three-winding transformers and a bipolar HVDC-LCC link supplied by three-winding transformers.

TABLE 5. Solution maximum deviations (order of magnitude) between PFPD and DGS (tolerance 10^{-8} p.u.) for the high and low load Italian transmission network.

	$\Delta\delta$ [°]	ΔV [%]
Low load	<1°	0.1
High load	<1°	0.1

TABLE 6. Circuital parameters of the HVDC links in the Italian transmission network.

	Configuration	Converter typology	Line Length λ [km]	Rated Power P_{DC} [MW]	DC Rated Voltage V_{DC} [kV]	AC Rated Voltage V_{AC} [kV]
Italy-France F.I.L.	monopolar	VSC	194,5	1200	±320	200
Italy-Montenegro MON.ITA	bipolar	LCC	445	600	±500	200
Italy-Italy SA.PE.I	bipolar	LCC	480,3	1000	±500	200
Italy-Greece GR.ITA	monopolar	LCC	317,2	500	400	160
Italy-France SA.CO.I.[a]	monopolar	LCC	385,2	300	200	80

[a] *The SA.CO.I. is a three-terminal HVDC link: it links the Italian peninsula to Sardinia passing through Corsica (France). In this study, this link is considered as a two-terminal HVDC link by considering the two active and reactive power absorption/injection at its extreme AC terminals (in Italy and in Sardinia).*

TABLE 7. AC nodal voltage comparisons between DGS and PFPD for the *Case E* network described in Sect. VII. Each voltage module is expressed in p.u., whereas each voltage angle in degree.

	DGS	PFPD
Bus 1	1.03000∠0°	1.03000∠0°
Bus 2	1.03000∠5.61001°	1.03000∠5.60976°
Bus 3	1.03000∠9.67599°	1.03000∠9.67574°
Bus 4	1.03000∠0.03910°	1.03000∠0.03885°
Bus 5	1.03000∠1.45916°	1.03000∠1.45891°
Bus 6	1.03000∠0.35846°	1.03000∠0.35821°
Bus 7	1.03000∠0.60569°	1.03000∠0.60594°
Bus 8	1.01505∠4.73767°	1.01505∠4.73742°
Bus 9	1.00336∠1.17033°	1.003364∠1.17008°
Bus 10	1.01466∠0.18214°	1.01466∠0.18239°
Bus 11	1.00859∠1.48588°	1.00859∠1.48563°
Bus 12	1.01578∠0.54413°	1.01578∠0.54438°
Bus 13	0.97416∠7.16761°	0.97416∠7.16786°
Bus 14	1.00354∠3.65883°	1.00354∠3.65909°
Bus 15	1.01021∠0.11431°	1.01021∠0.11456°
Bus 16	0.96384∠9.72989°	0.96384∠9.73014°
Bus 17	0.99886∠4.66011°	0.99886∠4.66036°
Bus 18	0.99311∠5.65340°	0.99311∠5.65365°

The tolerance of PFPD is set to 10^{-8} p.u.; a tolerance of the IRPE method equal to 100 V is chosen. Table 4 reports the maximum solution mismatches between PFPD and DGS computed by means of (32) and (33).

Such values confirm the very good agreement between the two computational methods and the capability of PFPD to treat different HVDC links inside the same network.

VIII. A REAL-WORLD APPLICATION OF PFPD: THE ITALIAN TRANSMISSION NETWORK

Due to its geographical collocation inside the synchronous ENTSO-E transmission system, the Italian network is connected with six nations by means of twenty-five interties [29].

TABLE 8. Rectifier parameters of the HVDC Link in the 18-Bus transmission network (*Case E*).

	RECTIFIER							
	V_{AC} (mod[p.u.], ang[deg])		V_{DC} [kV]		$\vartheta = \alpha$ [deg]		P_{loss_conv} [MW]	
	DGS	PFPD	DGS	PFPD	DGS	PFPD	DGS	PFPD
HVDC link (15-16)	0.95669∠ − 11.59431°	0.95670∠ − 11.59455°	151.681158	151.681158	11.10908	11.68605	1.17812	1.17813

TABLE 9. Inverter parameters of the HVDC link in the 18-Bus transmission network (*Case E*).

	INVERTER							
	V_{AC} (mod[p.u.], ang[deg])		V_{DC} [kV]		$\vartheta = \beta$ [deg]		P_{loss_conv} [MW]	
	DGS	PFPD	DGS	PFPD	DGS	PFPD	DGS	PFPD
HVDC link (15-16)	1.00598∠0.44325°	1.00598∠0.44300°	150.00000	150.00000	23.56232	22.93034	1.17812	1.17813

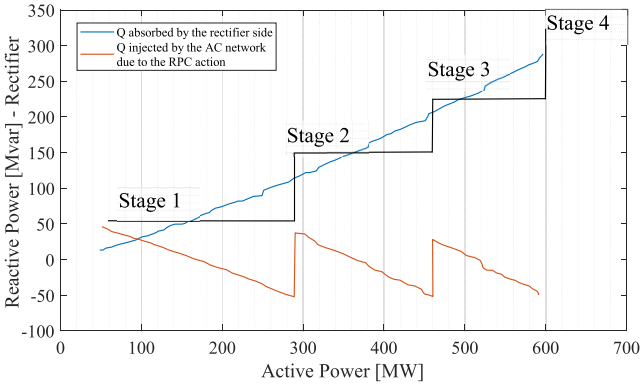

FIGURE 7. Experimental reactive power measurements as a function of the active power transmission for the MON.ITA HVDC link.

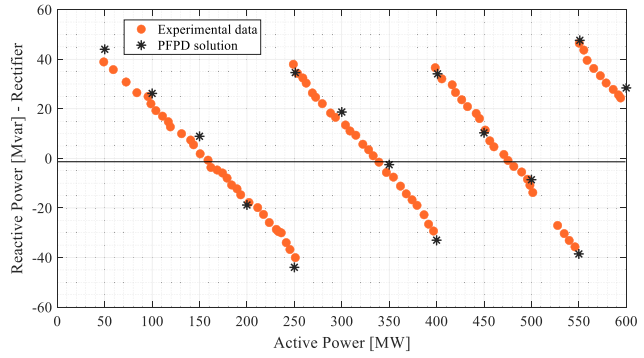

FIGURE 8. Comparison between experimental measurements and PFPD results for the MON.ITA HVDC link.

Four of these links are HVDC ones, whose characteristics are summarized in App. II. Another HVDC link connects the peninsular part of Italy with the Sardinia region (see in App. II the SA.PE.I link).

In order to test the industrial applicability of PFPD, a final validation is shown by considering the real-world Italian transmission network data.

Two different configurations of the Italian network are considered: a high load scenario and a low load scenario one. Their data are implemented both in Matlab environment and in DGS. The tolerance of the algorithm is set to 10^{-8} p.u. in both environments. In PFPD a tolerance for the IRPE method equal to 100 V is fixed. In Table 5 solution displacements in terms of voltage angles and magnitudes are presented. It is of note the good agreement between the two solutions: by considering both the scenarios, the maximum

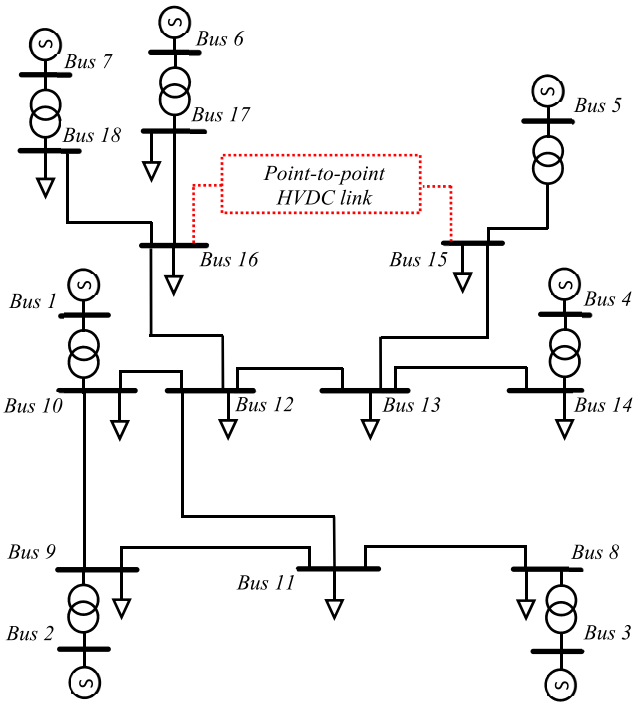

FIGURE 9. Single-phase diagram of the 18-bus fictitious network.

angle displacement computed for the voltage angle is 0.53° (found in the low load scenario) and 0.57° (found in high load scenario), whereas the order of magnitude of the maximum voltage displacement computed in both the scenarios is about 0.1%.

IX. HVDC-LCC RECTIVE POWER ABSORPTION: THE MON.ITA LINK CASE STUDY

In this section, an example of the applicability of PFPD to assess the impact of HVDC-LCC links in real power systems is shown. An experimental validation of PFPD by considering real steady-state measurements is assessed. It is known that, in HVDC-LCC links, the higher the transmitted active power, the higher the converter reactive power absorption [30] as inferable from (34):

$$Q_{AC} = \frac{P_{DC}}{V_{DC}\cos(\alpha)}\sqrt{(V_{DC} + R_{DC}I_{DC})^2 - (V_{DC}\cos(\alpha))}. \tag{34}$$

TABLE 10. DC line parameters of the HVDC link in the 18-Bus transmission network (*Case E*).

	DC LINE					
	I_{DC} [kA]		ΔV [%]		P_{loss_line} [MW]	
	DGS	PFPD	DGS	PFPD	DGS	PFPD
HVDC link (15-16)	1.97783	1.97783	1.12077	1.12077	3.32505	3.32505

TABLE 11. Rectifier parameters of the Italian transmission network HVDC links (Low load scenario).

	RECTIFIERS							
	V_{AC} (mod[p.u.], ang[deg])		V_{DC} [kV]		$\vartheta = \alpha$ [deg]		P_{loss_conv} [MW]	
	DGS	PFPD	DGS	PFPD	DGS	PFPD	DGS	PFPD
Italy-France F.I.L.	1∠0°	1∠0°	162.91121	162.91121	-	-	1.040847	1.040847
	1∠0°	1∠0°	162.91121	162.91121	-	-	1.040847	1.040847
	1∠0°	1∠0°	162.91121	162.91121	-	-	1.040847	1.040847
	1∠0°	1∠0°	162.91121	162.91121	-	-	1.040847	1.040847
Italy-France_Italy SA.CO.I.[a]	0.99159∠-1,87824°	0.99152∠-1.87841°	107.85873	107.85873	13.50808	13.622594	0.06652	0.06652
	0.99159∠-1,87824°	0.99152∠-1.87841°	107.85873	107.85873	13.50808	13.622594	0.06652	0.06652
Italy-Italy SA.PE.I	0.97854∠-1.02425°	0.97854∠-1.05632°	253.79223	253.79223	16.21074	16.21086	0.39127	0.39127
	0.97854∠-1.02425°	0.97854∠-1.05632°	253.79223	253.79223	16.21074	16.21086	0.39127	0.39127
	0.97854∠-1.02425°	0.97854∠-1.05632°	253.79223	253.79223	16.21074	16.21086	0.39127	0.39127
	0.97854∠-1.02425°	0.97854∠-1.05632°	253.79223	253.79223	16.21074	16.21086	0.39127	0.39127
Italy-Greece GR.ITA	0.98181∠-3.16262°	0.98181∠-3.16261°	203.08249	203.08249	16.80825	16.80751	0.54941	0.54941
	0.98181∠-3.16262°	0.98181∠-3.16261°	203.08249	203.08249	16.80825	16.80751	0.54941	0.54941
Italy-Montenegro MON.ITA	0.96598∠4.30960°	0.96593∠4.27431°	252.01693	252.01693	15.00000	15.00840	0.18540	0.18540
	0.96598∠4.30960°	0.96593∠4.27431°	252.01693	252.01693	15.00000	15.00840	0.18540	0.18540
	0.96598∠4.30960°	0.96593∠4.27431°	252.01693	252.01693	15.00000	15.00840	0.18540	0.18540
	0.96598∠4.30960°	0.96593∠4.27431°	252.01693	252.01693	15.00000	15.00840	0.18540	0.18540

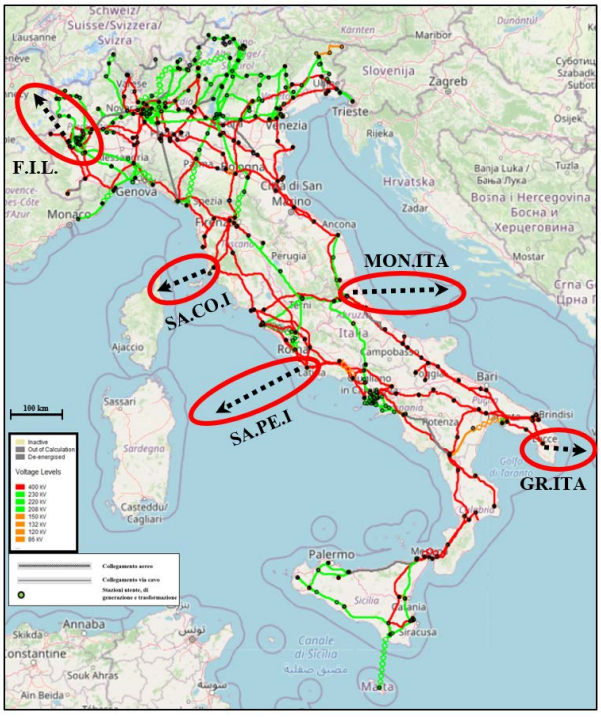

FIGURE 10. The Italian AC/DC network: the dotted arrows represent the HVDC links.

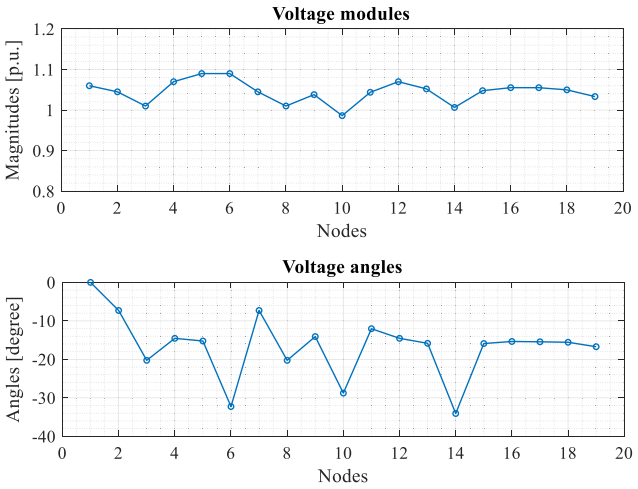

FIGURE 11. Power flow solution diagrams of the *Case E* network.

In order to maintain the reactive power absorption from the AC network inside a specified range, RPC logic is used [31], [32]. RPC logic basically insert/disconnect compensation devices in the PCC node to limit the reactive power absorption from the AC network. Fig. 7 shows the experimental measurements of an RPC test carried out during the commissioning of the MON.ITA HVDC link in 2019 [32]. These measurements are related to the rectifier side. To perform this test, the transmittable power is changed by step of 50 MW, and the RPC compensators are inserted/disinserted according to the active power transmitted. There are four reactive power compensators [32], whose combinations define different compensation stages depending on the transmitted active power.

It can be observed that the reactive power injected by the AC network (red line) is inside a ±50 Mvar range, so complying with the RPC specifications. The blue line represents the

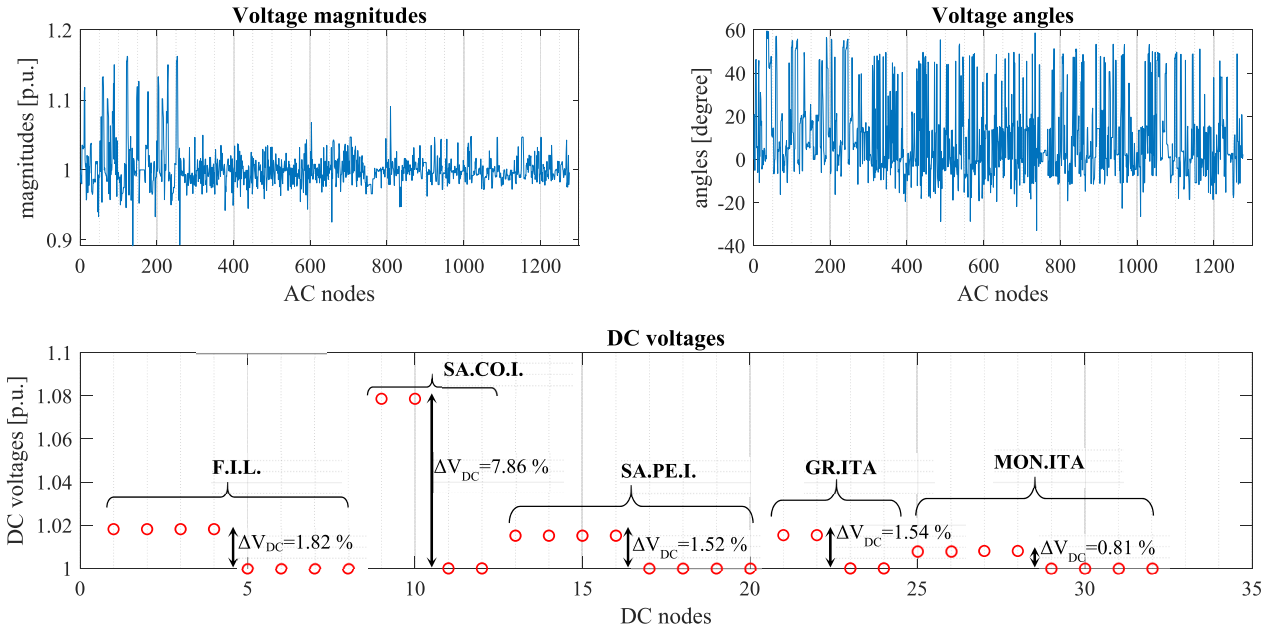

FIGURE 12. Power flow solution diagrams of the AC/DC Italian transmission network.

reactive power absorbed by the rectifier side: its requirement is guaranteed by both the AC networks and the AC compensation devices. The rated power of the adopted compensation stages is indicated by the black line.

The test configuration during the RPC test is modelled in PFPD, by considering the real Italian network data. The active power transmittable by the MON.ITA link is changed by considering 50 MW steps and by inserting the corresponding compensation stages. Fig. 8 illustrates the correlation between active and reactive power absorbed by the rectifier side of the MON.ITA link. A comparison between the experimental active/reactive measurements [32] and PFPD is shown. This case study confirms that PFPD results are consistent with the experimental measurements.

X. OPEN QUESTIONS

The present power flow procedure considers the two-terminal HVDC modelling by means of PV/PQ constraints. No HVDC multi-terminal configuration is considered.

Notwithstanding, some existing HVDC links could be connected to other ones: in the future, there could be more and more DC portions of radial/meshed transmission networks [2]. These DC network portions must be located inside the AC/DC boundaries which connect them to the AC network, also having integrated DC sources and DC loads. The authors hope that, in such future networks, new DC power flow constraints due to the converters can be fixed to set the power flow equations solving the problem. By starting from the DC network solutions, AC/DC boundaries could be set as PV/PQ constraints in order to study the AC network, similarly to the approach explained in this paper. Therefore, authors think that the presented power flow procedure can be further generalised to model HVDC multi-terminal links by means of PV/PQ constraints.

XI. CONCLUSION

The paper presents how PFPD can be suitably generalized to include HVDC-LCC/VSC links in the power flow of real and large AC/DC power systems. This matrix algorithm keeps all its performance in terms of CPU-time and convergence efficiency. HVDC-LCC/VSC are simultaneously considered by means of PQ and PV constraints: these ones follow the typical controls with the setpoints used in the different HVDC typologies. For HVDC-LCC, the reactive power to be included into PQ constraint are pre-estimated by an iterative procedure named as IRPE (which could be implemented also in N-R methods). Even if the DC networks are eliminated, after the convergence, all the DC quantities can be computed: transmission line and converter power losses, LCC converter firing angles etc. Filter behaviours are also considered at power frequency with their power losses.

Extensive comparisons with DIgSILENT PowerFactory also demonstrate the high level of accuracy of PFPD power flow solutions. Eventually, PFPD is efficiently applied to the real Italian grid with four HVDC-LCC and one HVDC-VSC links: some comparisons with measurements carried out during the real-time operation of Italy-Montenegro HVDC-LCC shows the power and accuracy of PFPD. Such open-access algorithm also plays and will play a key role for the planning and operation of the future Italian HVDC systems i.e., the Adriatic and Tyrrhenian links.

APPENDIX I: THE 18-BUS TEST NETWORK

The AC 18-bus test network used in this study is represented in Fig. 9. The different HVDC link typologies are inserted between nodes 15 and 16.

TABLE 12. Inverter parameters of the Italian transmission network HVDC links (Low load scenario).

	INVERTERS							
	V_{AC} (mod[p.u.], ang[deg])		V_{DC} [kV]		$\vartheta = \beta$ [deg]		P_{loss_conv} [MW]	
	DGS	PFPD	DGS	PFPD	DGS	PFPD	DGS	PFPD
Italy-France F.I.L.	1∠20.67016°	1∠20.67016°	160.00000	160.00000	-	-	1.071966	1.071966
	1∠20.67016°	1∠20.67016°	160.00000	160.00000	-	-	1.071966	1.071966
	1∠20.67016°	1∠20.67016°	160.00000	160.00000	-	-	1.071966	1.071966
	1∠20.67016°	1∠20.67016°	160.00000	160.00000	-	-	1.071966	1.071966
Italy-France-Italy SA.CO.I.[a]	0.97625∠3.12842°	0.97627∠3.0977°	100.00000	100.00000	18.53942	18.53294	0.06651	0.06651
	0.97625∠3.12842°	0.97627∠3.0977°	100.00000	100.00000	18.53942	18.53294	0.06651	0.06651
Italy-Italy SA.PE.I	0.97964∠3.12225°	0.97951∠3.14641°	250.00000	250.00000	19.11861	19.08927	0.39126	0.39126
	0.97964∠3.12225°	0.97951∠3.14641°	250.00000	250.00000	19.11861	19.08927	0.39126	0.39126
	0.97964∠3.12225°	0.97951∠3.14641°	250.00000	250.00000	19.11861	19.08927	0.39126	0.39126
	0.97964∠3.12225°	0.97951∠3.14641°	250.00000	250.00000	19.11861	19.08927	0.39126	0.39126
Italy-Greece GR.ITA	0.96570∠44.00425°	0.96568∠43.97344°	200.00000	200.00000	16.56962	16.56512	0.54941	0.54941
	0.96570∠44.00425°	0.96568∠43.97344°	200.00000	200.00000	16.56962	16.56512	0.54941	0.54941
Italy-Montenegro MON.ITA	0.98736∠1.86931°	0.98733∠1.87892°	250.00000	250.00000	20.37113	20.35603	0.18540	0.18540
	0.98736∠1.86931°	0.98733∠1.87892°	250.00000	250.00000	20.37113	20.35603	0.18540	0.18540
	0.98736∠1.86931°	0.98733∠1.87892°	250.00000	250.00000	20.37113	20.35603	0.18540	0.18540
	0.98736∠1.86931°	0.98733∠1.87892°	250.00000	250.00000	20.37113	20.35603	0.18540	0.18540

TABLE 13. DC line parameters of the Italian transmission network HVDC links (Low load scenario).

	DC LINE					
	I_{DC} [kA]		ΔV [%]		P_{loss_line} [MW]	
	DGS	PFPD	DGS	PFPD	DGS	PFPD
Italy-France F.I.L.	0.92897	0.92897	0.91788	0.91788	5.45719	5.45719
Italy-France-Italy SA.CO.I.[a]	1.39071	1.39071	7.85873	7.85873	21.85842	21.85842
Italy-Italy SA.PE.I	0.98506	0.98506	1.51689	1.51689	21.85843	21.85843
Italy-Greece GR.ITA	1.23103	1.23103	1.54125	1.54125	15.17852	15.17852
Italy-Montenegro MON.ITA	0.59520	0.59520	0.80678	0.80678	4.63040	4.63040

APPENDIX II: THE ITALIAN HVDC LINKS

In the Italian transmission network there are five HVDC links. Table 6 reports the main characteristics of these connections. For the Italian transmission network, two different scenarios are studied: a low load scenario and a high load scenario. In PFPD, the AC side terminals of the HVDC converters are modelled by considering the foreign networks as PV nodes, i.e., nodes in which the active power and voltage is scheduled. In DGS, instead, such nodes are modelled as external grids, which are specific blocks modelling entire networks as seen from one terminal.

There are several ways to set these external grids, however, in order to perform comparisons at the same conditions, they are modelled as PV nodes.

APPENDIX III: NUMERICAL RESULTS

In this appendix, some numerical results of the simulations described in Sect. VII and VIII are reported. The quantities represented in all the tables are rounded to five decimal places.

As an example, in Table 7 the comparisons between PFPD and DGS for the Case E (see Sect. VII) in terms of the AC nodal voltages are reported. Table 8, 9, and 10 report the computed quantities associated with the HVDC link between bus 15 and 16 (see Fig. 9). These tables show the significant quantities related to the HVDC link, and are subdivided into the rectifier, inverter, and DC line parts. It is worth noting from Table 7 to Table 10 the very good agreement between PFPD and DGS of the AC/DC results. In particular, the DC quantities assume the same value in both the environments: as it is said in Sect. VI, their computation is analytical. In particular, by means of (11) and (18), the value of the DC currents I_{DC} can be computed analytically, and so the computation of the DC voltages, and power losses. Therefore, the evaluation of the power losses introduced by the HVDC links can be estimated accurately by means of the approach described by (2)÷(9).

The above-mentioned consideration can be extended to the simulations of the Italian transmission network. By considering, as an example the low load scenario (see Sect. VIII for its description), Table 11, 12, and 13 report the computed quantities associated with the five HVDC links existing in the Italian network.

Fig. 11 and 12 synthetize the results of Table 7, and Tables 11/12 respectively. Fig. 11 represents the AC voltage magnitudes and angles of all the AC nodes of the Case E network (see Fig. 9). Fig. 12 shows the AC voltage magnitudes and angles, and the DC voltages of the five Italian HVDC links.

The p.u. DC voltages are computed by considering the DC base voltages of each HVDC link (which correspond to the inverter-side controlled voltages).

REFERENCES

[1] R. Benato, "A basic AC power flow based on the bus admittance matrix incorporating loads and generators including slack bus," *IEEE Trans. Power Syst.*, vol. 37, no. 2, pp. 1363–1374, Mar. 2022.
[2] D. V. Hertem, O. G. Bellmunt, and J. U. N. Liang, *HVDC Grids: For Offshore and Supergrid of the Future*. Hoboken, NJ, USA: Wiley, 2016.
[3] "Multidimensional issues in international electric power grid interconnections," United Nations Publication, United Nations Econ. Social Affairs, New York, NY, USA, Tech. Rep., 2006. [Online]. Available: http://www.un.org/esa/sustdev/publications/energy/interconnections.pdf
[4] C.-K. Kim, V. K. Sood, G.-S. Jang, S.-J. Lim, and S.-J. Lee, *HVDC Transmission: Power Conversion Applications in Power Systems*. Hoboken, NJ, USA: Wiley, 2009.
[5] M. Eremia, C.-C. Liu, and A.-A. Edris, *Advanced Solutions in Power Systems: HVDC, FACTS, and Artificial Intelligence*. Hoboken, NJ, USA: Wiley, 2016.
[6] R. Benato, S. D. Sessa, G. Gardan, and A. L'Abbate, "Converting overhead lines from HVAC to HVDC: An overview analysis," in *Proc. AEIT HVDC Int. Conf. (AEIT HVDC)*, May 2021, pp. 1–6.
[7] *HVDC Links in System Operations*, ENTSO-E, Brussels, Belgium, Dec. 2019.
[8] R. Benato, N. Crocamo, G. Gardan, G. M. Giannuzzi, C. Pisani, F. Sanniti, and R. Zaottini, "An original educational algorithm assessing the behaviours of angular frequency deviations of a multimachine system in small signal analysis," *IEEE Access*, vol. 9, pp. 18783–18800, 2021.
[9] T. Horigome and N. Ito, "Digital-computer method for the calculation of power flow in an a.c.-d.c. Interconnected power system," *Proc. Inst. Electr. Eng.*, vol. 111, no. 6, pp. 1137–1144, Jun. 1964.
[10] H. Sato and J. Arrillaga, "Improved load-flow techniques for integrated a.c.-d.c. Systems," *Proc. Inst. Electr. Eng.*, vol. 116, no. 4, pp. 525–532, Apr. 1969.
[11] G. Breuer, J. Luini, and C. Young, "Studies of large AC/DC systems on the digital computer," *IEEE Trans. Power App. Syst.*, vol. PAS-85, no. 11, pp. 1107–1116, Nov. 1966.
[12] N. G. Hingorani and J. D. Mountford, "Simulation of HVDC systems in AC load-flow analysis by digital computers," *Proc. Inst. Electr. Eng.*, vol. 113, no. 9, pp. 1541–1546, 1966.
[13] D. A. Braunagel, L. A. Kraft, and J. L. Whysong, "Inclusion of DC converter and transmission equations directly in a Newton power flow," *IEEE Trans. Power Appar. Syst.*, vol. PAS-95, no. 1, pp. 76–88, Jan. 1976.
[14] J. Arrillaga and P. Bodger, "AC-DC load flows with realistic representation of the convertor plant," *Proc. Inst. Electr. Eng.*, vol. 125, no. 1, pp. 41–46, Jan. 1978.
[15] H. E. Brown, G. K. Carter, H. H. Happ, and C. E. Person, "Power flow solution by impedance matrix iterative method," *IEEE Trans. Power App. Syst.*, vol. PAS-82, no. 65, pp. 1–10, Apr. 1963.
[16] H. W. Hale and R. W. Goodrich, "Digital computation or power flow–some new aspects," *Trans. Amer. Inst. Electr. Eng. III, Power App. Syst.*, vol. 78, no. 3, pp. 919–923, Apr. 1959.
[17] L. Gengyin, Z. Ming, H. Jie, L. Guangkai, and L. Haifeng, "Power flow calculation of power systems incorporating VSC-HVDC," in *Proc. Int. Conf. Power Syst. Technol. (PowerCon)*, vol. 2, Nov. 2004, pp. 1562–1566.
[18] K. Eriksson, T. Jonsson, and O. Tollerz, "Small scale transmission to AC networks by HVDC light," in *Proc. CEPSI Conf.*, Pattaya, Thailand, Nov. 1998, pp. 1–8.
[19] A. Pizano-Martinez, C. R. Fuerte-Esquivel, H. Ambriz-Pérez, and E. Acha, "Modeling of VSC-based HVDC systems for a Newton-Raphson OPF algorithm," *IEEE Trans. Power Syst.*, vol. 22, no. 4, pp. 1794–1803, Nov. 2007.
[20] G. Andersson. (Sep. 2008). Modelling and analysis of electric power systems. ETH Zürich. Accessed: Dec. 12, 2021. [Online]. Available: https://www.yumpu.com/en/document/read/4227429/modelling-and-analysis-of-electric-power-systems-eeh-eth-zurich
[21] J. Arrillaga, Y. H. Liu, and N. R. Watson, *Flexible Power Transmission: The HVDC Options, 1. Edizione*. Hoboken, NJ, USA: Wiley, 2007.
[22] J. Beerten, S. Cole, and R. Belmans, "Generalized steady-state VSC MTDC model for sequential AC/DC power flow algorithms," *IEEE Trans. Power Syst.*, vol. 27, no. 2, pp. 821–829, May 2012.
[23] *Rectifier/Inverter Technical Reference*, Tech. Document., DIgSILENT GmbH, Gomaringen, Germany, 2020.
[24] *PWM Converter Technical Reference*, Tech. Document., DIgSILENT GmbH, Gomaringen, Germany, 2020.
[25] X.-F. Wang, Y. Song, M. Irving, and A. C. di, "HVDC and FACTS," in *Modern Power Systems Analysis*. Boston, MA, USA: Springer, 2008, pp. 255–332.
[26] M. N. Undeland, W. P. Robbins, and N. Mohan, "Power electronics," in *Converters, Applications, and Design*. Hoboken, NJ, USA: Wiley, 1995.
[27] The China Electric Power Research Institute, "Steady-state characteristics of UHVDC transmission," in *UHV Transmission Technology*. Amsterdam, The Netherlands: Elsevier, 2018, pp. 429–468.
[28] J. Arrillaga and C. P. Arnold, *Computer Analysis of Power Systems: Arrillaga/Computer Analysis of Power Systems*. West Sussex, U.K.: Wiley, 1990.
[29] Terna Spa. *Interconnection Capacity With Foreign Countries*. Accessed: Feb. 4, 2022. [Online]. Available: https://www.terna.it/it/sistema-elettrico/mercato-elettrico/capacita-interconnessione-estero
[30] R. T. Pinto, A. C. Leon-Ramirez, M. Aragues-Penalba, A. Sumper, and E. Sorrentino, "A fast methodology for solving power flows in hybrid AC/DC networks: The European North Sea Supergrid case study," in *Proc. Int. Exhib. Conf. Power Electron., Intell. Motion, Renew. Energy Energy Manage. (PCIM Europe)*, May 2016, pp. 1–8.
[31] L. Cheng, Z. Zhang, S. Niu, X. Ke, and T. Huo, "Modeling of reactive power control system of HVDC," in *Proc. Asia–Pacific Power Energy Eng. Conf.*, Mar. 2010, pp. 1–4.
[32] G. Pecoraro, A. Pascucci, E. M. Carlini, M. Contu, M. Cortese, R. Gnudi, F. Allella, G. Bruno, and L. Michi, "HVDC link between Italy and montenegro: Impact of the commissioning on the real-time operation," in *Proc. AEIT Int. Annu. Conf. (AEIT)*, Sep. 2019, pp. 1–6.

ROBERTO BENATO (Senior Member, IEEE) was born in Venezia, Italy, in 1970. He received the Dr.-Ing. degree in electrical engineering from the University of Padova, in 1995, and the Ph.D. degree in power systems analysis, in 1999. In 2021, he was appointed as a Full Professor with the Department of Industrial Engineering, Padova University. He is the author of 200 papers and four books, edited by Springer, Wolters Kluwer, and China Machine Press. He has been a member of six Cigré Working Groups (WGs) and the Secretary of two Joint WGs, and a member of IEEE PES Substations Committee. Since 2014, he has been a nominated member of IEC TC 120 "Electrical Energy Storage (EES) Systems" in the WG 4 "Environmental issues of EES systems." He is also a Corresponding Member of Cigré WG B1.72 "Cable rating verification 2nd part." Since 2018, he has been elevated to the grade of CIGRÉ Distinguished Member. He is a member of Italian AEIT.

GIOVANNI GARDAN (Member, IEEE) was born in Padua, Italy, in 1995. He received the B.S. degree in energy engineering and the Dr.-Ing. degree in electrical engineering from the University of Padova, in 2017 and 2020, respectively, where he is currently pursuing the Ph.D. degree in industrial engineering. His research interests include electrical energy transmission, high voltage AC/DC system modeling, and computer analysis of large power systems. He is a member of IEEE Power & Energy Society and a Young Member of both Cigrè and AEIT.